COLLEGE OF ENGINEERING

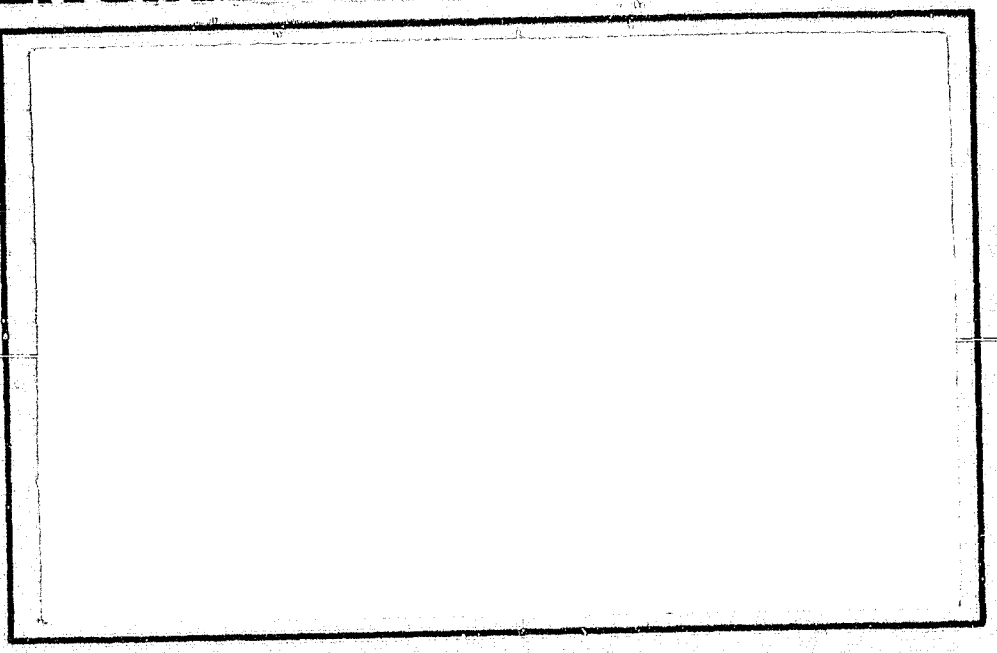

VIRGINIA POLYTECHNIC INSTITUTE AND STATE UNIVERSITY

BLACKSBURG, VIRGINIA

College of Engineering
Virginia Polytechnic Institute and State University
Blacksburg, VA 24061

VPI-E-81-4 March 1981

Calculations of the Room-Temperature Shapes of Unsymmetric Laminates

Michael W. Hyer[1]

Department of Engineering Science and Mechanics
NASA Cooperative Agreement NCCI-15 Interim Report No. 24
Prepared for: John G. Davis, Jr., Head
Materials Processing and Applications Branch
National Aeronautics and Space Administration
Langley Research Center
Hampton, Virginia 23665

[1]Associate Professor of Engineering Science and Mechanics
Virginia Polytechnic Institute and State University
Blacksburg, Virginia 24061

Preface

The enclosed report is a copy of a paper submitted for publication in the Journal of Composite Materials. The issuing of this report is not intended to duplicate the Journal's publication effort. This report is intended to accelerate the dissemenation of information resulting from investigations of advanced composite materials.

Abstract

The cured shape of unsymmetric laminates do not always conform to the predictions of classical lamination theory. Classical lamination theory predicts the room-temperature shapes of all unsymmetric laminates to be a saddle. Experimental observations, however, indicate some unsymmetric laminates have cylindrical room-temperature shapes. In addition, some unsymmetric laminates, exhibit two stable room-temperature configurations, both cylindrical. This paper presents a theory which explains these characteristics. The theory is based on an extension of classical lamination theory which accounts for geometric nonlinearities. A Rayleigh-Ritz approach to minimizing the total potential energy is used to obtain quantitative information regarding the room-temperature shapes of square T300/5208 $[0_2/90_2]_T$ and $[0_4/90_4]_T$ graphite-epoxy laminates. It is shown that, depending on the thickness of the laminate and the length of the side of the square, the saddle shape configuration is actually unstable. For values of length and thickness that render the saddle shape unstable, it is shown that two stable cylindrical shapes exist. The predictions of the theory are compared with existing experimental data.

Introduction

Most calculations used to predict the response of laminates to static, dynamic, or thermal loadings are based on what has become to be known as classical lamination theory [1], [2], [3]. This is a linear theory and is based on the following major assumptions:

(1) the displacements are continuous throughout the laminate,

(2) the Kirchhoff hypothesis regarding undeformed normals is assumed to be valid,

(3) the strain-displacement relationship is linear,

(4) the material is linearly elastic, and

(5) the through-the-thickness stresses are small in comparison to the in-plane stresses.

The theory smears the individual lamina properties by integrating the constitutive equations through the thickness of the laminate. As a result of this integration, force and moment resultants are defined. In addition, the well-known A, B, and D matricies are defined. While this theory is quite capable of accurately predicting static deflections, natural vibration frequencies and mode shapes, buckling loads and mode shapes, and thermal expansion coefficients of laminates, there are physical situations for which the theory fails to predict the correct answer. Two situations of note are: the inability of the theory to predict the response of thicker laminates, and; its inability to explain the behavior of laminates near edges. The former problem has been studied by several investigators [4], [5] and satisfactory corrections to the theory have been obtained. The latter problem is now a classic and has been studied by many individuals, at least for the case of the

straight free-edge. A survey of the edge problem has been put forth in [6].

There appears to be another situation for which classical lamination theory fails to give the correct answer. Specifically, it appears the theory is unable to correctly predict the room-temperature shapes of thin unsymmetric laminates. Hyer [7] has documented the room-temperature shapes of several families of unsymmetric laminates and found that the room-temperature shapes of some thin unsymmetric laminates are closely approximated by right circular cylinders. In addition, some thin laminates have two room-temperature cylindrical shapes. These results are in contrast to the predictions of the classical theory. The classical theory predicts the room-temperature shapes of all unsymmetric laminates to be a saddle with unique (single-valued) curvature characteristics. Specifically, Hyer found that 100 x 100 mm and 150 x 150 mm $[0_2/90_2]_T$ T300/5208 graphite-epoxy laminates cured to become cylindrical at room temperature. In addition, they exhibited a snap-through or oil-canning phenomenon. The cylindrical shape could be snapped into another cylindrical shape which had the same characteristics as the first shape. However, the second cylinder was oriented perpendicular to the first cylinder and the curvature of the second cylinder was of opposite sign. Hyer showed that thicker (say, 8-layer) 100 x 100 mm unsymmetric laminates conformed to the predictions of the theory.

To explain the behavior of unsymmetric laminates, it was assumed that it would be necessary to incorporate a nonlinear effect into classical lamination theory. The existence of two room-temperature shapes

(i.e. the two cylinders) essentially ruled out a linear extension to the theory since a linear extension would lead to the prediction of a unique shape, albiet perhaps not a saddle shape. Furthermore, since the out-of-plane deflections of the unsymmetric laminates were on the order of many laminate thicknesses, geometric nonlinearities were felt to be an important effect. Thus, in an effort to explain the behavior of unsymmetric laminates, classical lamination theory was extended to include geometric nonlinearities through the strain-displacement relationship. This extension was applied to the analysis of the $[0_n/90_n]_T$, n=1,2,... family of laminates. This family was chosen for study because this class of laminates always exhibits a snap-through phenomenon, there is data available for different thickness $[0_n/90_n]_T$ laminates, and due to some of the A_{ij}, B_{ij}, and D_{ij} terms being zero with this family, the algebra associated with this family of laminates is simplier than the algebra associated with other families. The analysis of the room-temperature shapes of this family of laminates is the subject of this paper. The paper traces the development of the analysis which successfully predicts the existence of two room-temperature cylindrical shapes, and compares the predictions with the available data.

Problem Formulation

Since a problem formulation which includes geometric nonlinearities would result in nonlinear governing equations, it was assumed from the beginning that obtaining a closed-form exact solution for the unsymmetric laminate problem would be difficult and not really necessary. The occurence of the cylindrical shape is so prevalant with thin laminates that it was hypothesised that one is dealing with a fundamental

phenomenon rather than some higher order effect. Thus any good approximate theory would reveal the mechanics of the problem. The problem is idealized as follows. A cured laminate (and uncured prepreg) is flat at the elevated curing temperature, fig. 1a. As the laminate cools, it is assumed it is free from any external mechanical forces which produce net work. It is assumed the out-of-plane deflections develop only because of the differences in thermal expansion properties of the individual lamina. This idealization ignores the effects of any mechanical constraints the autoclaving and vacuum bagging process may exert on the laminate. Upon cooling, the laminate deforms into one of the shapes given by figs. 1b, c and d. Of these shapes, the one that actually occurs is the one associated with a minimum of the total potential energy. The shape scenario given by figs. 1b, c and d includes the saddle shape observed for the thicker laminates and predicted by the classical theory, and the two possible cylindrical shapes observed for the thinner laminates. It is assumed that in attaining these shapes, geometric nonlinearities are important.

Since it is assumed external tractions are not important during the cooling process, the total potential energy, including the effects of thermal expansion, is given by [8],

$$W = \int_{Vol} W dVol, \tag{1}$$

$$W = \frac{1}{2} C_{ijkl} e_{ij} e_{kl} - \beta_{ij} e_{ij} \Delta T, \tag{2}$$

where W equals the strain energy density. The C_{ijkl} are the elastic constants of the material and the β_{ij} are coefficients related to the elastic constants and the coefficients of thermal expansion of the material. Both the elastic properties and the thermal expansion coeffi-

cients are assumed to be temperature-independent. The e_{ij} are the strains in the material and ΔT is the temperature change in the material due to cooling from curing. In eq. (2), since the problem is a plane-stress formulation, i and j assume the values 1 and 2. These values are not directly related to the principal material directions of the lamina, but rather, 1 and 2 are associated with the x and y directions of the laminates (see fig. 1). Thus the following relations apply:

$$e_{11} = \varepsilon_x^\circ - z\frac{\partial^2 w}{\partial x^2}, \tag{3}$$

$$e_{22} = \varepsilon_y^\circ - z\frac{\partial^2 w}{\partial y^2}, \tag{4}$$

$$e_{12} = \varepsilon_{xy}^\circ - z\frac{\partial^2 w}{\partial y \partial x}, \tag{5}$$

with

$$\varepsilon_x^\circ = \frac{\partial u^\circ}{\partial x} + \frac{1}{2}\left(\frac{\partial w}{\partial x}\right)^2 \tag{6}$$

$$\varepsilon_y^\circ = \frac{\partial v^\circ}{\partial y} + \frac{1}{2}\left(\frac{\partial w}{\partial y}\right)^2, \text{ and} \tag{7}$$

$$\varepsilon_{xy}^\circ = \frac{1}{2}\left(\frac{\partial u^\circ}{\partial y} + \frac{\partial v^\circ}{\partial x} + \left(\frac{\partial w}{\partial x}\right)\left(\frac{\partial w}{\partial y}\right)\right). \tag{8}$$

As usual, z=0 is the midplane of the laminate. The quantity u° is the laminate midplane displacement in the x-direction, v° is the laminate midplane displacement in the y-direction, and w is the out-of-plane displacement of the midplane.

Equations (6) - (8) represent the principal departure from classical lamination theory and include the usual approximations associated with thin-plate theory when employing the nonlinear geometric effects in

the strain-displacement relations. These approximations assume the elongation and shearing strains and the squares of the rotations are the same order of magnitude and this order is small compared to unity [9], [10].

For a laminate the C_{ijkl}'s can be related to the $\bar{Q}_{ij}$'s, the reduced stiffnesses, and the β_{ij}'s can be related to the $\bar{Q}_{ij}$'s and α_x, α_y, and α_{xy}, the laminate thermal expansion coefficients in the x-y coordinate system. Expanding eq. 2 yields

$$W = \frac{1}{2}\bar{Q}_{11}e_{11}^2 + \bar{Q}_{12}e_{11}e_{22} + 2\bar{Q}_{11}e_{12}^2 + \frac{1}{2}\bar{Q}_{22}e_{22}^2 - (\bar{Q}_{11}\alpha_x + \bar{Q}_{12}\alpha_y)e_{11}\Delta T - (\bar{Q}_{12}\alpha_x + \bar{Q}_{22}\alpha_y)e_{22}\Delta T \quad . \tag{9}$$

(α_{xy}=0 for this family of laminates.) The problem has now been reduced to one of finding the deformation u°, v°, and w as functions of x and y which, through eqs. (2) - (9), minimize eq. (1). As previously mentioned, approximate solutions to u°, v°, and w are sought. In seeking realistic approximate solutions, two basic assumptions are made. First, it is assumed that even in attaining the cylindrical shape, the midplane elongation strains, ε_x° and ε_y°, do not vary much from the linear prediction (i.e. ε_x° and ε_y° independent of x and y). Second, it is assumed that to the order of the nonlinearity considered here, the midplane shear strains are negligible i.e. $\varepsilon_{xy}^\circ = 0$. Since for $[0_n/90_n]_T$ laminates classical lamination theory predicts ε_{xy}° to be zero and ε_x° and ε_y° to be constant, these two assumptions could be lumped into one by saying it is assumed that even in attaining the cylindrical shapes, magnitude of the midplane strains do not vary much from the predictions of the classical theory. However, for rationalizing the choice of the

functional form of the approximate solutions, the two issues are separated.

It is assumed w(x,y) is of the form

$$w(x,y) = \frac{1}{2}\,(ax^2 + by^2)\ , \tag{10}$$

a and b being constants. With this functional form for w, both the classical lamination solution, a = -b, and either of the two cylindrical shapes, fig. 1c and d, can be approximated. For fig. 1c the solution can be $a \neq 0$, $b = 0$ while for fig. 1d the solution can be $a = 0$, $b \neq 0$. Using the kinematic assumptions regarding the midplane strains, ε_x°, ε_y°, and ε_{xy}°, the approximate solutions for u° and v° are given by

$$u^\circ(x,y) = cx - \frac{a^2x^3}{6} - \frac{abxy^2}{4} \tag{11}$$

$$v^\circ(x,y) = dy - \frac{b^2y^3}{6} - \frac{abx^2y}{4}\ , \tag{12}$$

c and d being constants. Using eqs. (11) and (12) in eqns. (6) - (8) yields

$$\varepsilon_x^\circ = c - \frac{aby^2}{4} \tag{13}$$

$$\varepsilon_y^\circ = d - \frac{abx^2}{4} \tag{14}$$

$$\varepsilon_{xy}^\circ = 0. \tag{15}$$

Note that if it were not required to have ε_{xy}° be zero, the third term in each of eqs. (11) and (12) would not need to be included and then the second term in eqs. (13) and (14) would not appear. However, with the $[0_n/90_n]_T$ family, it is felt in-plane shear strains are impossible and this is the prime factor in choosing the functional form for u° and v°.

At this point a, b, c and d are considered as generalized coordi-

nates and are to be determined. The problem of finding a minimum for the total potential energy, W, becomes a problem of finding solutions to the values of a, b, c, and d so that the first variation of W is zero, i.e.

$$\delta W = \left(\frac{\partial W}{\partial a}\right)\delta a + \left(\frac{\partial W}{\partial b}\right)\delta b + \left(\frac{\partial W}{\partial c}\right)\delta c + \left(\frac{\partial W}{\partial d}\right)\delta d \equiv 0 \ . \tag{16}$$

This variation is done with all the assumptions in the Introduction with the exception of (3).

Calculations Associated with the Solution

The x-y-z coordinate system in fig. 1 is assumed to be situated such that at the elevated curing temperature the laminate is defined by the region

$$\begin{aligned} -L_x/2 \leq x \leq L_x/2 \\ -L_y/2 \leq y \leq L_y/2 \\ -h/2 \leq z \leq h/2 \ . \end{aligned} \tag{17}$$

With these limits on the spatial variables and with the various material properties involved, eq. (1) takes the form

$$W = \int_{x=-L_x/2}^{L_x/2} \int_{y=-L_y/2}^{L_y/2} \int_{z=-h/2}^{h/2} W(a,b,c,d,\bar{Q}_{ij},\alpha_x,\alpha_y,\Delta T,x,y,z)\,dx\,dy\,dz. \tag{18}$$

The involved, but straight-forward, process of substituting eqs. (10) and (13) - (15) into eqs. (3) - (5), substituting these results into eq. (9), performing the spatial integrations in eq. (18), and finally taking the first variation, eq. (16), leads to an equation of the form:

$$\begin{aligned} \delta W = f_1(a,b,c,d)\delta a + f_2(a,b,c,d)\delta b + \\ f_3(a,b,c,d)\delta c + f_4(a,b,c,d)\delta d = 0 \ . \end{aligned} \tag{19}$$

Equation (19) immediately leads to four equations:

$$f_1(a,b,c,d) = -C_1cb + C_2ab^2 + 2C_3ab - B_{11}c + D_{11}a - C_4cb + 2C_5ab^2 - C_6db + D_{12}b - C_7db + C_8ab^2 + C_9b^2 + (L_y^2/48)N_x^Tb + M_x^T + (L_x^2/48)N_y^Tb = 0 , \tag{20}$$

$$f_2(a,b,c,d) = -C_1ac + C_2a^2b + 2C_3a^2 - C_4ac + 2C_5a^2b + D_{12}a - C_6da - C_7da + C_8a^2b + 2C_9ab - B_{22}d - D_{22}b + (L_y^2/48)N_x^Ta + (L_x^2/48)N_y^Ta + M_y^T = 0 , \tag{21}$$

$$f_3(a,b,c,d) = A_{11}c - C_1ab - B_{11}a + A_{12}d - C_4ab - N_x^T = 0 , \tag{22}$$

$$f_4(a,b,c,d) = A_{12}c - C_6ab - B_{22}b + A_{22}d - C_7ab - N_y^T = 0 . \tag{23}$$

The constants C_1 - C_9 are defined in the Appendix and A_{ij}, B_{ij} and D_{ij} have the familiar definitions associated with laminates. The other definitions used in eqs. (20) - (23) are,

$$N_x^T = \Delta T \int_{-h/2}^{h/2} (\bar{Q}_{11}\alpha_x + \bar{Q}_{12}\alpha_y)dz , \tag{24}$$

$$N_y^T = \Delta T \int_{-h/2}^{h/2} (\bar{Q}_{12}\alpha_x + \bar{Q}_{22}\alpha_y)dz , \tag{25}$$

$$M_x^T = \Delta T \int_{-h/2}^{h/2} (\bar{Q}_{11}\alpha_x + \bar{Q}_{12}\alpha_y)zdz , \tag{26}$$

$$M_y^T = \Delta T \int_{-h/2}^{h/2} (\bar{Q}_{12}\alpha_x + \bar{Q}_{22}\alpha_y) z dz \ . \tag{27}$$

These quantities are immediately recognizable as the effective in-plane thermal loads, N_x^T and N_y^T, and the effective thermal moments, M_x^T and M_y^T. It should be noted that when $L_x = L_y = 0$, the coefficients C_1 through C_9 are all zero and eqs. (20) - (23) reduce to the equations of classical lamination theory.

Solution of Equations, Numerical Results

Solutions to eqs. (20) - (23) were obtained by solving eqs. (22) and (23) for c and d in terms of a and b and substituting these relations into eqs. (20) and (21). Thus eqs. (20) and (21) become coupled cubic equations for the quantitites a and b. These two resulting equations have the characteristics of being able to be reduced to a single cubic equation for either a or b. Such an equation would have either one or three real roots. This reduction approach was not used, however, and eqs. (20) and (21), in terms of a and b, were solved numerically. Solutions were obtained for several laminates using elastic and thermal expansion properties of T300/5208 graphite-epoxy. It was assumed the curing temperature of T300/5208 is 177° C (350° F) and that the laminates are cooled to a room temperature of 21° C (70° F). The material properties used in the calculations were:

E_1 = 181 GPa (26.2×10^6 psi)

E_2 = 10.3 GPa (1.49×10^6 psi)

ν_{12} = 0.28

G_{12} = 7.17 GPa (1.04×10^6 psi)

$\alpha_1 = -0.106 \times 10^{-6}/^\circ C$ $(-0.059 \times 10^{-6}/^\circ F)$

$\alpha_2 = 25.6 \times 10^{-6}/^\circ C$ $(14.2 \times 10^{-6}/^\circ F)$

The elastic properties were taken from [2] while the thermal expansion coefficients were taken from [11]. Solutions were obtained for square laminates ($L_x=L_y=L$) ranging from 0 to 150 mm in length on a side. Two thicknesses were considered, $[0_2/90_2]_T$ and $[0_4/90_4]_T$. Experimental data were available for some checking of these two thickness cases. Figure 2 shows the characteristics of the predicted room-temperature shapes of the $[0_2/90_2]_T$ laminate and fig. 3 shows the characteristics for the thicker laminate. Each figure illustrates the effect of the size of the laminate, L, on the room temperature shapes.

Immediately obvious from the figures is the existence of three possible room-temperature shapes of the laminate if the lengths of the sides are greater than some critical value. For both laminates, at L=0 the room-temperature shape is the saddle predicted by classical lamination theory, a=-b. This solution is denoted by point A on figs. 2 and 3. As the sides of the laminate increase in length, say to L=25 mm for the $[0_2/90_2]_T$ laminate of fig. 2, the shape is still predicted to be a saddle but one which is shallower than the one predicted by the classical theory. As the lengths of the sides increase, the saddle shape is still predicted to exist but it gets shallower and shallower. At some critical length, the solution bifurcates. For the thinner laminate the critical length is 35 mm while for the thicker laminate the critical length is 71 mm. The bifurcation point is denoted as B on the figures. For lengths greater than the critical length, three room temperature shapes, each represented by a different branch on the figures, can

possibly exist. These branches are denoted as BC, BD, and BE on the figures. Branch BD represents a continuation of the saddle shape (a=-b) but the other two branches represent a radical departure from a saddle shape. Branch BC represents a shape which has a large curvature in the x-direction and practically no curvature in the y-direction, fig. 1c. On the other hand, branch BE represents a shape which has a large curvature in the y-direction and very little curvature in the x-direction, fig. 1d. The shapes associated with these latter branches can be considered cylindrical because as the laminate gets larger, i.e. L increases, the one curvature asymptotically approaches zero while the other curvature asymptotically approaches a non-zero constant value. As seen from the figures, the latter two branches have certain symmetry characteristics. These symmetry characteristics are such that for a given length, the values of a and b associated with branch BC are equal, respectively, to the values of -b and -a associated with branch BE.

Figures 2 and 3 show both laminates exibit similar behavior. There are differences however. The two main differences are that the curvatures for the thicker laminate are less than the curvatures for the thinner laminate, and, the critical length for the thicker laminate is greater. Thus, compared to a $[0_2/90_2]_T$ laminate, a $[0_4/90_4]_T$ can be made larger before the triple-shape phenomenon occurs.

Stability of the Predicted Shapes

With multiple solutions to a nonlinear problem, the question arises as to the stability of the various solutions. If any of the solutions do not represent a stable solution, those solutions will not be physically realizable. Equating the first variation of the total potential

energy to zero yields equilibrium positions of the laminate which either maximize or minimize the total energy. For stable equilibrium, the total potential energy must be mimimized. Thus, for stable equilibrium the second variation of the total potential energy, $\delta^2 W$, must be positive definite. From stability theory [12] for this discretized system, stability of the equilibrium positions for the laminate is possible if and only if the following matrix of coefficients is positive definite:

$$\begin{vmatrix} \frac{\partial f_1}{\partial a} & \frac{\partial f_1}{\partial b} & \frac{\partial f_1}{\partial c} & \frac{\partial f_1}{\partial d} \\ \frac{\partial f_2}{\partial a} & \frac{\partial f_2}{\partial b} & \frac{\partial f_2}{\partial c} & \frac{\partial f_2}{\partial d} \\ \frac{\partial f_3}{\partial a} & \frac{\partial f_3}{\partial b} & \frac{\partial f_3}{\partial c} & \frac{\partial f_3}{\partial d} \\ \frac{\partial f_4}{\partial a} & \frac{\partial f_4}{\partial b} & \frac{\partial f_4}{\partial c} & \frac{\partial f_4}{\partial d} \end{vmatrix} . \qquad (28)$$

For a given equilibrium solution at a given length, e.g. the saddle solution of the triple-valued solution at L=100 mm, each element of the matrix is evaluated numerically by substituting in the values of a, b, c, and d corresponding to that solution. If each of the principal minors of the matrix are positive definite, the matrix is positive definite and the solution corresponds to a stable equilibrium solution. Otherwise the solution corresponds to an unstable equilibrium solution. Using this scheme for the solutions shown in figs. 2 and 3, it was found that the saddle solutions corresponding to the single-valued solutions, segments AB in the figures, were <u>stable</u>. On the other hand, the saddle solutions corresponding to the triple-valued solutions, segments BC in the figures, were <u>unstable</u>. The other two branches of the triple-

valued solutions, segments BD and BE, represent stable solutions. Physically this means that for square laminates of the $[0_2/90_2]_T$ family, if the length of the sides of the laminate exceed 35 mm, the saddle shape does not exist. Instead, two cylindrically shaped equilibrium configurations exist. If the laminate is from the thicker $[0_4/90_4]_T$ family, the length of a side must exceed 71 mm before the saddle-shape equilibruim configuration disappears and dual cylindrical shapes appear. The fact that two stable cylindrical equilibrium solutions are predicted to exist is felt to be significant since it correlates well with the the reported snap-through phenomena associated with these types of laminates.

Experimental Results

Shown on fig. 2 are two data points. These points correspond to the curvatures of cylindrical $[0_2/90_2]_T$ laminates as measured by Hyer. Figure 3 shows one data point. This point corresponds to the curvature of a $[+45_4/-45_4]_T$ saddle-shaped T300/5208 graphite-epoxy laminate as measured by Pagano and Hahn [13]. The comparison between magnitudes of the predicted and experimentally measured curvatures is fair. More importantly, however, the character of the measured shapes, i.e. cylindrical or saddle, compares well with the predictions. For the 150 x 150 mm laminate shown in fig. 2, only the major curvature of 11 laminates were measured in the original work and the average curvature and the range are shown here arbitrarily as a y-direction curvature, b. These curvatures could have just as easily been called an x-direction curvature. In this case the experimental data would have been associated with the variable a. Also the major curvature from the one 100 x 100 mm

specimen is also arbitrarily associated with the y-direction curvature. For the data point in fig. 3, the curvature of the specimen was never measured directly. The out-of-plane deflection across the diagonals of a 63.5 mm (2.50 in.) square laminate was measured and the curvature was computed from this measure. Again this single curvature measurement was arbitrarily associated with the variable b.

It should be noted in fig. 2 that the x-direction curvature for the 100 x 100 mm laminate was measured to be slightly negative. The theory predicts this curvature to be slightly positive. The reason for the descrepancy is not clear. However, it is not felt to be due to measuring error in the experimental determination of curvature. This points needs further investigation.

Discussion

Despite the lack of large amounts of quantitative experimental data to compare with the complete range of the numerical predictions, the results of the work reported here are quite encouraging. First, the theoretical calculations predict the disappearance of the saddle shape, a phenomenon observed by many investigators. Second, the snap-through or appearance of two stable equilbrium states is predicted, another phenomenon observed by investigators. Finally, the transition from stable single-valued saddle solutions to stable cylindrical solutions is linked with a size effect. The figures show that both the thickness of the laminate and the length of the side determine whether the cylindrical shape exists or whether the saddle shape exists. This investigator, as well as others, has felt a size effect exists in unsymmetric laminates and the model put forth here lends some credence to that

notion.

While the predictions presented here exhibit all the important features associated with unsymmetric laminates, several comments are in order before closure. First, the solution presented here is a one-term Galerkin, or Rayleigh-Ritz, solution. Thus the solution is, as with all one-term Galerkin solutions, over-constrained. This deficiency can be remedied by using more terms, and hence more generalized coordinates, in the assumed functional forms for u°, v°, and w. Modifying the current approach this way would probably change the numerical values associated with each solution branch of figs. 2 and 3 but not the main features of bifurcation and triple-solution. Second, the effects of moisture absorption, viscoelastic relaxation, or any other mechanism that alters the internal stress state of the laminate is felt to be important for laminates with lengths near the critical length. Alteration of the internal stress state most likely influences the numerical value of the critical length. Thus a laminate sized just above the critical length could, with time, actually be sized just below the critical length due to any of the above mentioned time-dependent effects. Related to this is the fact that unsymmetric laminates sized near their critical length could exhibit "strange" behavior, requiring practically no force to snap them from one shape to another. More than likely, these multiple shapes would be some barely stable combination of shallow cylinders and shallow saddles.

Finally, the analysis presented here is based on symmetric curing (symmetric about the $z=0$ plane) of the laminate and, as noted above, the lack of any effects to alter the internal stress state over and above

that due to temperature change during the cool-down from curing. The result is that for lengths greater than the critical length, two simiiliar shapes are possible. Each of these shapes has the same possibility of actually occurring. However, any external perturbation which is unsymmetric with respect to the midplane will cause one or the other of the two possible cylindrical shapes to be favored. Such a perturbation could be unsymmetric curing (due to unsymmetric cooling), unsymmetric moisture absorbtion, or any other process over which our control is limited. Thus in reality it may require, for example, more force to snap the cylinder of fig. 1c to the cylinder of fig. 1d than it does to make the reverse snap.

Appendix

$$C_1 = A_{11}L_y^2/48 \; ; \qquad C_2 = A_{11}L_y^4/1280$$

$$C_3 = B_{11}L_y^2/48 \; ; \qquad C_4 = A_{12}L_x^2/48$$

$$C_5 = A_{12}L_x^2L_y^2/2304 \; ; \qquad C_6 = A_{12}L_y^2/48$$

$$C_7 = A_{22}L_x^2/48 \; ; \qquad C_8 = A_{22}L_x^4/1280$$

$$C_9 = B_{22}L_x^2/48$$

The coefficients A_{11}, A_{12}, A_{22}, B_{11} and B_{22} have the familiar definitions associated with classical lamination theory.

References

1. Jones, R. M., Mechanics of Composite Materials, McGraw-Hill Book Co., New York, 1975, Ch. 4.

2. Tsai, S. W. and Hahn, H. T., Introduction to Composite Materials, Technomic Publishing Co., Inc., Westport, CT 06880, 1980, Chs. 4, 5 and 6.

3. Agarwal, B. D. and Broutman, L. J., Analysis and Performance of Fiber Composites, John Wiley and Sons, New York, 1980, Ch. 5.

4. Whitney, J. M., "Shear Correction Factors for Orthotropic Laminates Under Static Load," J. Applied Mech., Trans. ASME, vol. 40, Series E, no. 1, 1973, p. 302-304.

5. Whitney, J. M. and Pagano, N. J., "Shear Deformations in Heterogeneous Anisotropic Plates," J. Applied Mech., Trans. ASME, vol. 37, Series E, no. 4, 1970, p. 1031-1036.

6. Salamon, N. J., "An Assessment of the Interlaminar Stress Problem in Laminated Composites," J. Composite Materials, to appear.

7. Hyer, M. W., "Some Observations on the Cured Shape of Thin Unsymmetric Laminates," submitted to J. Composite Materials.

8. Fung, Y. C., Foundations of Solid Mechanics, Prentice-Hall Inc., Englewood Cliffs, NJ, 1965, p. 354.

9. Chia, C.-Y. Nonlinear Analysis of Plates, McGraw-Hill, Inc., New York, 1980, Ch. 1.

10. Novozhilov, V. V., Foundations of the Nonlinear Theory of Elasticity, Graylock Press, Rochester, NY, 1953, p. 83.

11. Bowles, D. E., Post, D., Herakovich, C. T. and Tenny, D. R., Thermal Expansion of Composites Using Moiré Interferometry, Virginia Polytechnic Institute and State University, College of Engineering Report, VPI-E-80-19, 1980.

12. Simitses, G. J., An Introduction to the Elastic Stability of Structures, Prentice-Hall, Inc., Englewood Cliffs, NJ, 1976, p. 8-14.

13. Pagano, N. J. and Hahn, H. T., "Evaluation of Composite Curing Stresses," Composite Materials: Testing and Design, 4th Conference, ASTM STP 617, 1977, p. 317-329.

Fig. 1 Laminate Shapes: (a) at the elevated curing temperature, and at room-temperature, (b) a saddle shape, (c) a cylindrical shape, (d) another cylindrical shape.

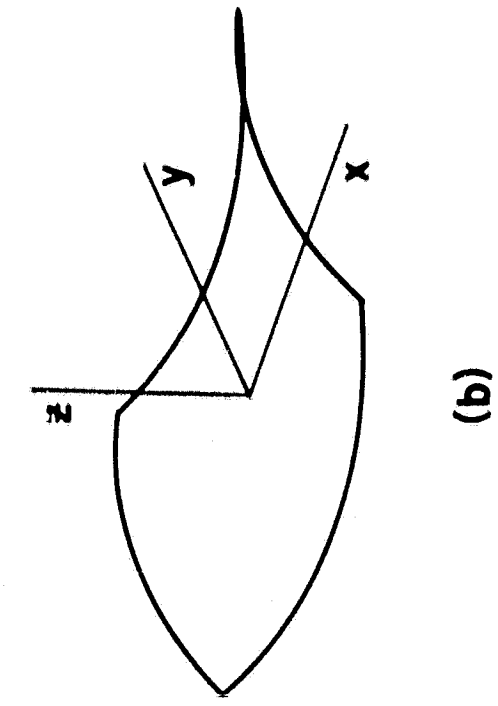

(b)

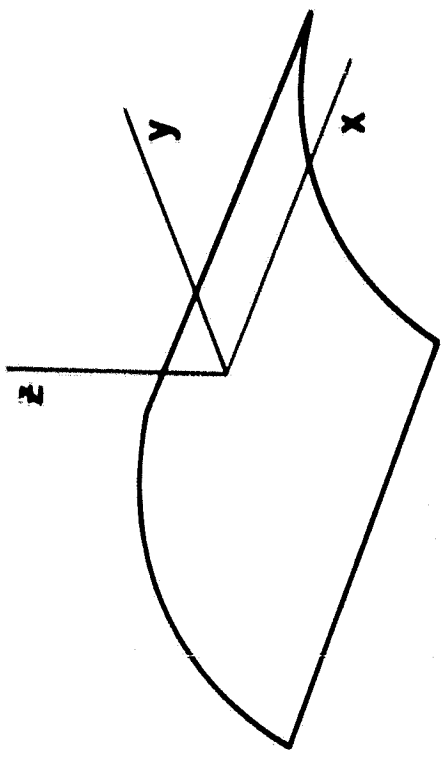

(d)

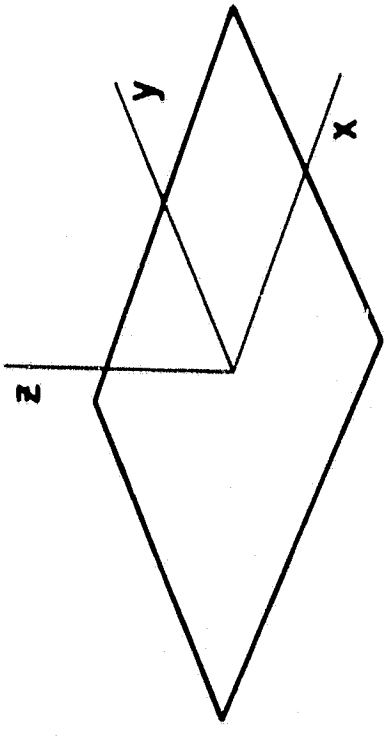

(a)

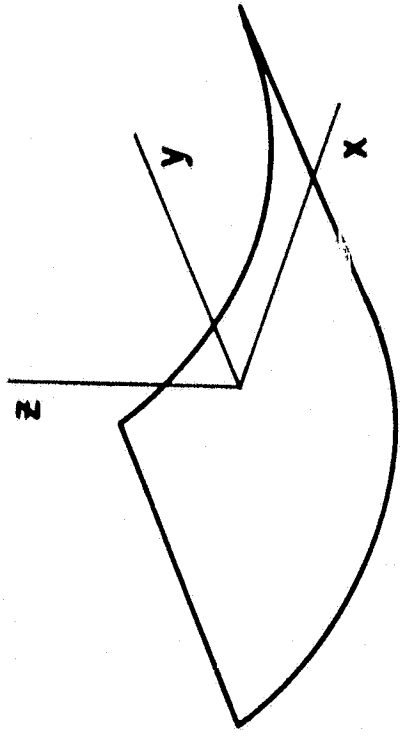

(c)

Fig. 2 Room-temperature shapes of square $[0_2/90_2]_T$ T300/5208 graphite-epoxy laminates

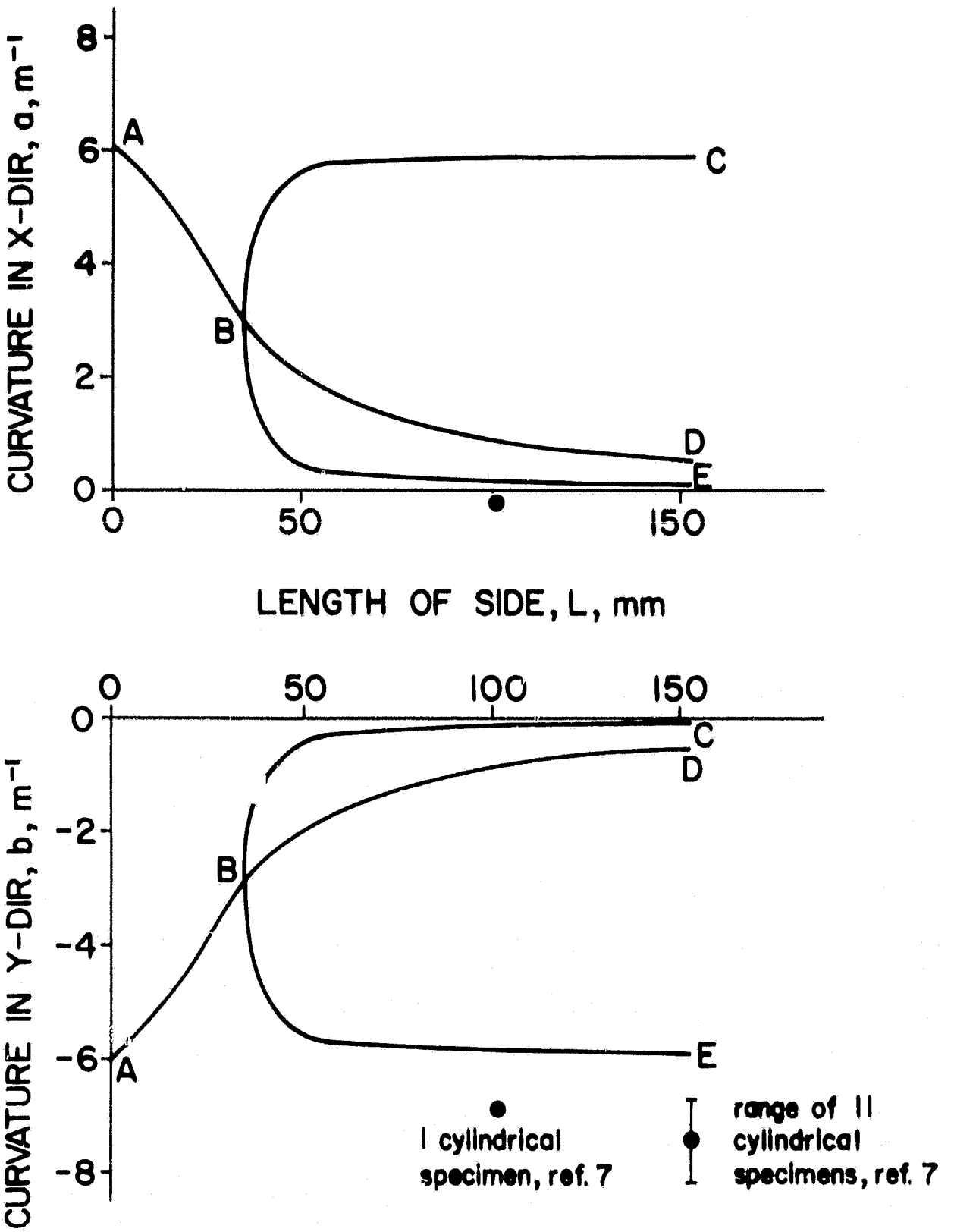
CURVATURE IN X-DIR, a, m⁻¹
8
6
4
2
0
A
B
C
D
E
0
50
150
LENGTH OF SIDE, L, mm
0
50
100
150
0
-2
-4
-6
-8
CURVATURE IN Y-DIR, b, m⁻¹
A
B
C
D
E
1 cylindrical specimen, ref. 7
range of 11 cylindrical specimens, ref. 7

Fig. 3 Room-Temperature shapes of square $[0_4/90_4]_T$ T300/5208 graphite-epoxy laminates

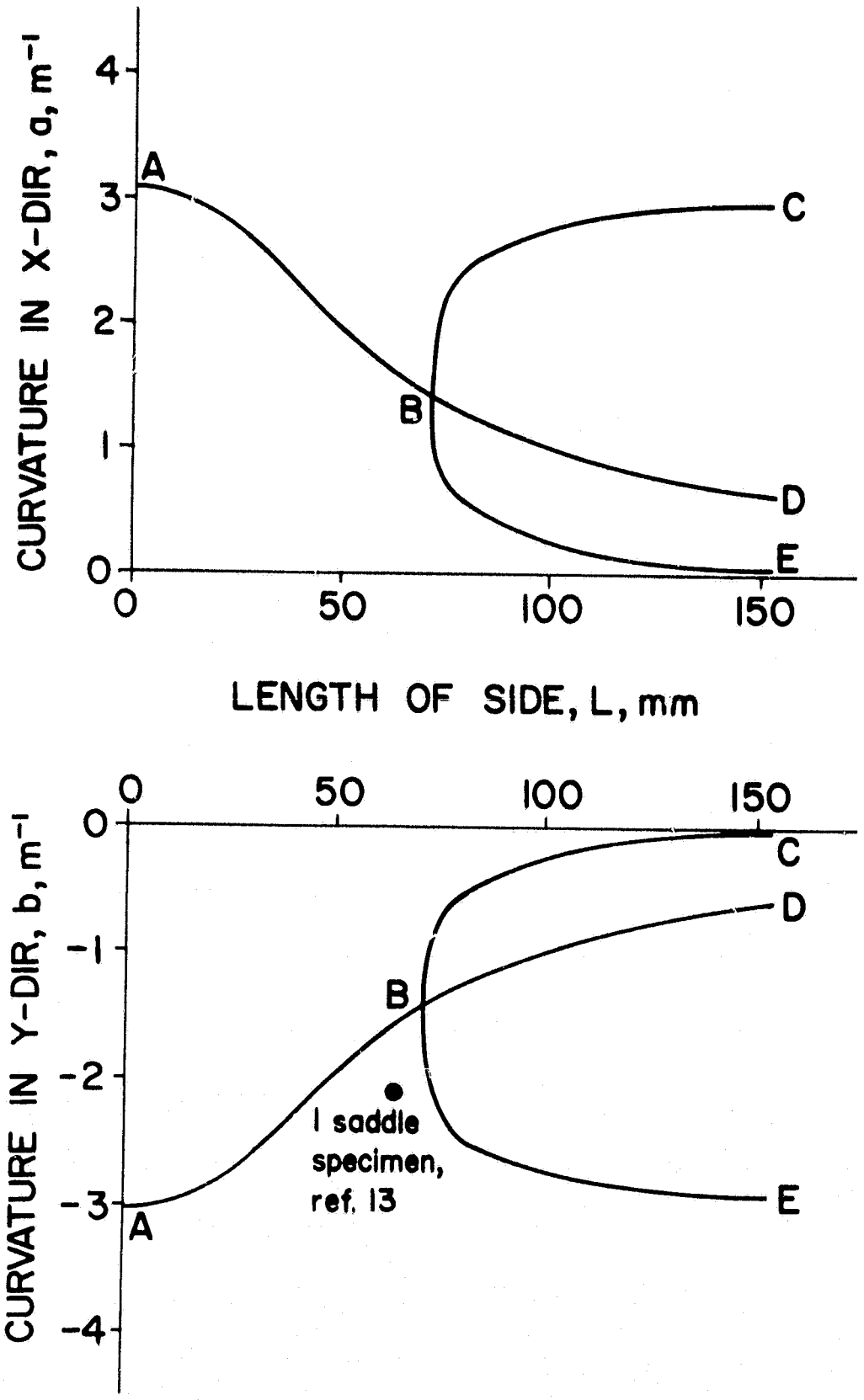
CURVATURE IN X-DIR, a, m⁻¹
4
3
2
1
0
A
B
C
D
E
0
50
100
150
LENGTH OF SIDE, L, mm
CURVATURE IN Y-DIR, b, m⁻¹
0
-1
-2
-3
-4
1 saddle
specimen,
ref. 13

Prof. Donald F. Adams
Dept. Of Mechanical Engineering
University Of Wyoming
Larmie, WY 82070

Dr. N. R. Adsit
General Dynamics Convair
P.O. Box 80837
San Diego, CA. 92138

Winfield H. Arata, Jr.
4414 Countrywood Drive
Santa Maria, CA 93455

Dr. Clifford J. Astill
Solid Mechanics Program
National Science Foundation
1800 G St. N.W.
Washington, D.C.

AVCO, Systems Division
Subsystems & Meth. Structures
201 Lowell Street
Wilmington, MA. 01887

Dr. J. A. Bailie
D81-12 Bldg. 154
Lockheed Missiles & Space Co,Inc
1111 Lockheed Way
Sunnyvale, CA. 94088

Dr. Charles W. Bert, Director
School Of Aerospace, Mechanical
& Nuclear Engineering
The University Of Oklahoma
Norman, Oklahoma 73069

Dr. C. M. Blackmon
NSWC, Code K21
Dahlgren, VA 22448

Mr. Richard Boitnott
Mail Stop 190
Nasa-Langley Research Center
Hampton, VA. 23665

Mr. David Bowles
Mail Stop 188B
NASA-Langley Research Center
Hampton, Va. 23665

Dr. H. F. Brinson
ESM Dept.
Virginia Tech
Blacksburg, VA. 24061

Mr. Ernie Brooks
Code 1844
DTMSRDC
Bethesda, MD 20084

Dr. Micharl F. Card
Mail Stop 190
NASA-Langley Research Center
Hampton, VA 23665

Dr. C. Chamis
NASA-Lewis Research Center
2100 Brook Park Rd.
Cleveland, Ohio 44135

Dr. Paul A. Cooper
Mail Stop 190
NASA-Langley Research Center
Hampton, Va. 23665

Dr. Frank Crossman
Lockheed Research Lab
Org. 52-41, Bldg. 204
3251 Hanover Street
Palo Alto, CA. 94304

Dr. I. M. Daniel, Manager
IIT Research Institute
10 West 35 Street
Chicago, IL. 60616

Dr. John R. Davidson
Mail Code 188E
MD-Structural Integrity Branch
Langley Research Center
Hampton, VA. 23665

Dr. John G. Davis, Jr.
Mail Stop 188A
Langley Research Center
Hampton, VA. 23665

Mr. Jerry W. Deaton
Mail Stop 188A
NASA-Langley Research Center
Hampton, VA. 23665

Mr. H. Benson Dexter
Mail Stop 188A
NASA-Langley Research Center
Hampton, VA. 23665

Mr. O. Earl Dhonau
Section 2-53400
Vought Corp.
P.O. Box 5907
Dallas, TX. 75222

Dr. M. F. Duggan
52-33/205/2
Lockheed Palo Alto Lab.
3251 Hanover St.
Palo Alto, Ca. 94304

Prof. John C. Duke, Jr.
ESM Dept.
Virginia Tech
Blacksburg, VA. 24061

Prof. George J. Dvorak
Civil Engineering
University of Utah
Salt Lake City, UT. 84112

Dr. Wolf Elber
Mail Stop 188E
NASA-Langley Research Center
Hampton, VA. 23665

Mr. Dave Erb
Aero & Ocean Engr. Dept.
Virginia Tech
Blacksburg, VA. 24061

Mr. Gary L. Farley
Mail Stop 188A
NASA-Langley Research Center
Hampton, VA. 23665

Mr. Larry Fogg
Lockheed-California
Dept. 7572, Bldg. 63, Plant A1
P.O. Box 551
Burbank, CA. 91520

Dr. R. L. Foye
USAMRDL
SAUDLAS (207-5)
Moffet Field, CA. 94035

Dr. D. Frederick
ESM Dept.
Virginia Tech
Blacksburg, VA. 24061

Mr. Samuel P. Garbo
McDonnell Aircraft Co.
Bldg. 34, Post 350
St. Louis, MO. 63166

Mr. Ramon Garica
Mail Stop 190
NASA-Langley Research Center
Hampton, VA. 23665

Prof. Jim Goree
Dept. of Mechanical Engr.
Clemson University
Clemson, S.C. 29631

Dr. Login B. Greszczuk
McDonnell Douglas Astr. Co.
5301 Bolas Avenue
Huntington Beach, CA. 92647

Dr. O. Hayden Griffin, Jr.
Bendix Advanced Technology Ctr.
9140 Old Annopolis Road
Columbia, MD 21045

Mr. Glen C. Grimes
Dept. 3852/82
Northrop Corp., Aircraft Div.
3901 West Broadway
Hawthorne, CA. 90250

Dr. H. T. Hahn
Washington University
St. Louis, MO. 63130

Dr. J. C. Halpin
Flight Dynamics Lab
Wright-Patterson AFB
Ohio 45433

Professor Z. Hashin
School of Engineering
Solid Mech. Materials & Struc.
Tel Aviv University
Tel Aviv, Israel

Dr. R. A. Heller
ESM Dept.
Virginia Tech
Blacksburg, VA. 24061

Dr. E. G. Henneke
ESM Dept.
Virginia Tech
Blacksburg, VA. 24061

Prof. Carl T. Herakovich
Laboratoire de Mecanique
des Solides
Ecole Polytechnique
91128 Palaiseau cedex, FRANCE

Professor Phil Hodge
107 Aeronautical Engr. Bldg.
University of Minnesota
Minneapolis, MN 55455

Dr. K. E. Hofer
IIT Research Institute
10 West 35 Street
Chicago, Illinois 60616

Mr. Edward A. Humphreys
Materials Science Corporation
Blue Bell Office Campus
Blue Bell, PA. 19422

Dr. Michael W. Hyer
ESM Dept.
Virginia Tech
Blacksburg, VA. 24061

Dr. Eric R. Johnson
ESM Dept.
Virginia Tech
Blacksburg, VA. 24061

Dr. N. J. Johnson
Mail Stop 226
NASA-Langley Research Center
Hampton, VA. 23665

Dr. M. P. Kamat
ESM Dept.
Virginia Tech
Blacksburg, VA. 24061

Dr. Keith T. Kedward
1768 Granite Hills Dr.
El Cajon, CA. 92021

Mr. John M. Kennedy
Mail Stop 188E
NASA-Langley Research Center
Hampton, VA. 23665

Mr. Eric Klang
ESM Dept.
Virginia Tech
Blacksburg, VA. 24061

Mr. James F. Knauss
Northrop Corporation
3901 West Broadway
Dept. 3852/82
Hawthorne, CA. 90250

Dr. Ronald D. Kriz
Dept. Com. NBS Bldg. 2
Boulder, CO. 80302

Dr. S. V. Kulkarni
1342 Lawrence Livermore Lab
P. O. Box 808
Livermore, Ca. 94550

Dr. Trent R. Logan
Mgr. Structures, Design, Dev.
Boeing Commercial Airplane Co.
P.O. Box 3707 - M.S. 3M-23
Seattle, WA. 98124

Dr. M. R. Louthan
Materials Engineering
Virginia Tech
Blacksburg, VA. 24061

Mr. Vic Mazzio
General Electric Co.
P.O. Box 8555
Bldg. 100, Rm. M4018
Philadelphia, PA. 19101

Dr. Martin M. Mikulas
Mail Stop 190
NASA-Langley Research Center
Hampton, VA. 23665

Mr. J. Steve Mills
A3-220 13-3 McDonald Douglas
5301 Bolsa Avenue
Huntington Beach, CA 96247

Dr. D. H. Morris
ESM Dept.
Virginia Tech
Blacksburg, VA. 24061

Mr. Anya Nagarkar
Material Sciences Corp.
Blue Bell Office Campus
Blue Bell, PA. 19422

NASA Scientific & Technical
Information Facility
P.O. Box 8757
Baltimore/Washington Inter. Air.
Baltimore, MD. 21240

Mr. Michael Nemeth
ESM Dept.
Virginia Tech
Blacksburg, VA. 24061

Newman Library
Virginia Tech

Mr. David A. O'Brien
5902 Kingsford Pl.
Bethesda, MD 20034

Dr. Donald W. Oplinger
Army Materials & Mechanics
Research Center
Department of the Army
Watertown, MA. 02171

Dr. Nicholas J. Pagano
WPAFB/MBM
Wright Patterson AFB
Ohio 45433

Mr. Michael Parin
3M Co., 3M Center
Bldg. 230-1F
St. Paul, MN. 55101

Dr. Nicholas Perrone, Director
Structural Mechanics Program
Department of the Navy
Office of Naval Research
Arlington, VA. 22217

Prof. T. H. H. Pian
Mass. Inst. of Tech.
Dept. of Aero. & Astr.
Cambridge, MA. 02139

Mr. Marek-Jerzy Pindera
ESM Dept.
Virginia Tech
Blacksburg, VA. 24061

Dr. R. Byron Pipes
Dept. of Mech. & Aero. Engr.
107 Evans Hall
University of Delaware
Newark, DE. 19711

Prof. Robert Plunkett
Dept. Aero & Eng. Mech.
Aero 107
University of Minnesota
Minneapolis, MN. 55455

Dr. K. L. Reifsnider
ESM Dept.
Virginia Tech
Blacksburg, VA. 24061

Dr. Gary D. Renieri
McDonnell Douglas Astro. Co-East
P.O. Box 516
Bldg. 106, Level 4, Post C-5
St. Louis, MO. 63166

Dr. Michael W. Renieri
McDonnell Aircraft Co.
Bldg. 34, Post 350
St. Louis, MO. 63166

Dr. Larry Roderick
Mail Stop 188E
NASA-Langley Research Center
Hampton, VA. 23665

Dr. B. W. Rosen
Materials Science Corporation
Blue Bell Office Campus
Blue Bell, PA. 19422

Dr. R. E. Rowlands
Dept. of Engineering Mechanics
University of Wisconsin
Madison, WI. 53706

Dr. Edmund F. Rybicki
Mechanical Engineering Dept.
The Univ. of Tulsa
Tulsa, OK. 74104

Mr. Harminder Saluja
Boeing Vertol Company
Structural Technology
P.O. Box 16858
Philadelphia, PA. 19142

Dr. J. Wayne Sawyer
Mail Stop 190
NASA-Langley Research Center
Hampton, VA. 23665

Dr. George P. Sendeckyj
Structures Division
Air Force Flight Dynamics Lab.
Wright-Patterson AFB
Ohio 45433

Mr. Steven M. Serabian
28 Berkeley Drive
Chelmsford, MA. 01824

Mr. John S. Short, Jr.
ESM Dept.
Virginia Tech
Blacksburg, VA. 24061

Mr. Mark J. Shuart
Mail Stop 188
NASA-Langley Research Center
Hampton, VA. 23665

Dr. J. R. Stafford
B.F. Goodrich
500 S. Main St.
D/6145, B/10-E
Akron, Ohio 44318

Dr. James H. Starnes, Jr.
Mail Stop 190
NASA-Langley Research Center
Hampton, VA. 23665

Prof. Yehuda Stavsky
Gerard Swope Prof. of Mech.
Technion-Israel Inst. of Tech.
Technion City, Haifa, Israel

Dr. W. W. Stinchcomb
ESM Dept.
Virginia Tech
Blacksburg, VA. 24061

Dr. Darrel R. Tenney
Mail Code 188B
MD-Materials Research Branch
Langley Research Center
Hampton, VA. 23665

Dr. S. W. Tsai
Nonmetallic Materials Division
Air Force Materials Laboratory
Wright-Patterson AFB
Ohio 45433

Dr. J. R. Vinson
Dept. of Mech. & Aero. Engr.
107 Evans Hall
University of Delaware
Newark, DE. 19711

Mr. M. E. Waddoups
General Dynamic Corp.
Fort Worth, TX 76101

Prof. A. S. Wang
Mechanical Engineering
Drexel University
Philadelphia, PA. 19104

Prof. S. S. Wang
Dept. Theoretical & Applied
Mechanics
University of Illinois
Urbana, IL. 61801

Dr. T. A. Weisshaar
School of Aero. & Astro.
331 Grissom Hall
Purdue Univ.
West Lafayette, IN. 47907

Dr. J. M. Whitney
Nonmetallic Materials Division
Air Force Materials Laboratory
Wright-Patterson AFB
Ohio 45433

Dr. Ernest G. Wolff
The Aerospace Corp.
P.O. Box 92957
Los Angeles, CA. 90009

Dr. Edward Wu
Lawrence Livermore Lab.
University of California
Box 808, L-338
Livermore, CA. 94550

Mr. Thomas A. Zeiler
School of Aero. & Astro.
Grissom Hall
Purdue Univ.
West Lafayette, IN. 47907

Dr. Carl H. Zweben
General Electric Co.
Space Division
P.O. Box 8555
Philadelphia, PA. 19101